Grading the Severity of Arteriolosclerosis from Retinal Arterio-venous Crossing Patterns

Liangzhi Li[1], Manisha Verma[1], Bowen Wang[1], Yuta Nakashima[1],
Ryo Kawasaki[2], and Hajime Nagahara[1]

[1] Institute for Datability Science (IDS), Osaka University, Osaka 565-0871, Japan
`{li, mverma, n-yuta, nagahara}@ids.osaka-u.ac.jp`
`bowen.wang@is.ids.osaka-u.ac.jp`
[2] Graduate School of Medicine, Osaka University, Osaka 565-0871, Japan
`ryo.kawasaki@ophthal.med.osaka-u.ac.jp`

Abstract

Background and Objective: The status of retinal arteriovenous crossing is of great significance for clinical evaluation of arteriolosclerosis and systemic hypertension. As an ophthalmology diagnostic criteria, Scheie's classification has been used to grade the severity of arteriolosclerosis. In this paper, we propose a deep learning approach to support the diagnosis process, which, to the best of our knowledge, is one of the earliest attempts in medical imaging.
Methods: The proposed pipeline is three-fold. First, we adopt segmentation and classification models to automatically obtain vessels in a retinal image with the corresponding artery/vein labels and find candidate arteriovenous crossing points. Second, we use classification model to validate the true crossing point. At last, the grade of severity for the vessel crossings is classified. To better address the problem of label ambiguity and imbalanced label distribution, we propose a new model, named multi-diagnosis team network (MDTNet), in which the sub-models with different structures or different loss functions provide different decisions. MDTNet unifies these diverse theories to give the final decision with high accuracy.
Results: Our severity grading method was able to validate crossing points with precision and recall of 96.3% and 96.3%, respectively. Among correctly detected crossing points, the kappa value for the agreement between the grading by a retina specialist and the estimated score was 0.85, with an accuracy of 0.92. The numerical results demonstrate that our method can achieve a good performance in both arteriovenous crossing validation and severity grading tasks.
Conclusions: By the proposed models, we could build a pipeline reproducing retina specialist's subjective grading without feature extractions. The code is available for reproducibility[3].

Keywords: Medical Imaging · Retina Images · Artery Hardening · Deep Learning.

---

[3] The code is available at `https://github.com/conscienceli/MDTNet`
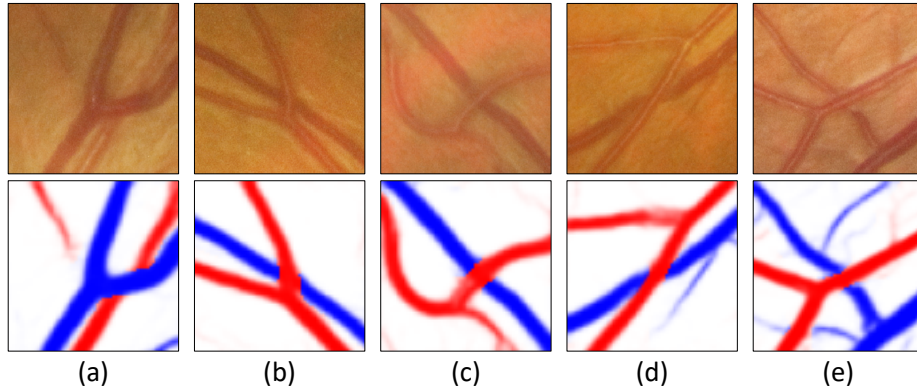
Fig. 1. Typical examples of our prediction targets. Images in the first and second rows are raw retinal patches and automatically-generated vessel maps with manually-annotated artery/vein labels, respectively. Red represents arteries while blue represents veins. (a) is false crossing (the vein runs above the artery), while (b)–(e) are for *none*, *mild*, *moderate*, and *severe* grades, respectively. Note that even the state-of-the-art segmentation techniques cannot capture caliber narrowing, therefore, the arteriioloscleroses are not very obvious in the vessel maps.

1   Introduction

The ophthalmologic examination has been regarded as an important routine for detecting not only multiple eye-related diseases but also ocular manifestations of many anomalies in the systemic circulatory system and the nervous system [1]. Among these detectable anomalies, arteriolosclerosis is critical yet asymptomatic, of which diagnosis may be mostly conducted by medical specialists, requiring vast experiences while mostly subjective qualitative observations.

Assessment of arteriovenous crossing points in retinal images provides rich cues for quick screening of arteriosclerosis and even for classifying them into different severity grades [2]. The assessment is based on some diagnostic criteria, for example, Scheie's classification [3], as shown in Figs. 1(b)–(e). The grades are described as follows: (i) *none* (no anomaly observed); (ii) *mild* (slight shrink in the caliber at venular edges); (iii) *moderate* (narrowed caliber at a single venular edge); and (iv) *severe* (narrowed caliber at both venular edges).

However, human graders are subjective and usually with different levels of experiences, and there has been a criticism in the low reproducibility of severity grading, which makes grading results from human graders unreliable for clinical practice, screening, and clinical trials [4]. Also, considering the ever-increasing demand for ophthalmologic examination, computer-aided diagnosis (CAD) is extremely helpful for quick screening. Yet, retinal image analysis for CAD is a challenging task due to the high complexity of the vessel system and huge visual differences among retinal images.

In fact, most researchers in this area have been focusing on preliminary tasks, such as vessel segmentation [5,6,7], artery/vein classification [8,9,10], etc. A few works address higher-level tasks [11,4], mostly on top of vessel segmentation, such as vessel width measurement, vessel-to-vessel ratio calculation, etc. However, they usually struggle in actual diagnoses: Firstly, vessel segmentation in retinal images *per se* is a challenging task. The vessel maps in Fig. 1(c)–(e), which are produced by the state-of-the-art segmentation model [12], cannot capture such deformation. This may imply that deformation is too minor to be captured by segmentation models, although such kind of segmentation-based approaches is a typical solution for automatic severity grading. Secondly, the existing methods detect arteriovenous crossing points by applying some morphological operators to vessel maps [13]. This approach may not be accurate enough to find crossing points that satisfy diagnostic requirements. For example, we can only use crossing points at which the artery is above the vein for diagnosis, and Fig. 1(a) is not a diagnostic crossing point since the artery goes below the vein.

Instead of fully relying on segmentation results, we propose a multi-stage approach, in which segmentation results are used only for finding crossing point candidates, and actual prediction of the severity grade is done for an image patch around each crossing point after validating if the crossing point is an actual and informative one. To the best of our knowledge, this is the first work proposing a fully-automatic methodology aiming at grading arteriolosclerosis through the joint detection and analysis of retinal crossings.

Another issue in our severity grading task, which is very common in medical imaging, is the imbalanced label distribution. Most patients in our dataset have the slightest signs (*none* and *mild*) of arteriolosclerosis while only a few patients suffer from the *severe* grades of artery hardening. Also, the boundaries among different severity labels are not always obvious, making accurate diagnosis challenging.

Inspired by the concept of the multidisciplinary team [14], which strives to make a comprehensive assessment of a patient, we propose a multi-diagnosis team network (MDTNet) in this paper to address the imbalanced label distribution and label ambiguity problems at the same time. MDTNet can combine the features from multiple classification models with different structures or different loss functions. Some of the underlying models in MDTNet use the class-balanced focal loss [15] to handle hard or rare samples, of which the original version requires hyperparameter tuning, while MDTNet can utilize the advantage of the focal loss without tuning its hyperparameters.

Our main contribution is two-fold: (i) We propose a whole pipeline for an automatic method for severity grading of artery hardening. Our method can find and validate possible arteriovenous crossing points, for which the severity grade is predicted. (ii) We design a new model, MDTNet, which uses the focal loss to address the problem of data ambiguity and unbalance. Interestingly, our experimental results show that by ensembling multiple models' features, our model without hyperparameter tuning outperforms baselines with the focal loss.

2   Dataset

We built a vessel crossing point dataset extracted from our retinal image database with $1,440$ images in the size of $5,184 \times 3,456$ pixels, which are captured by the CR-2 AF Digital Non-Mydriatic Retinal Camera (Canon, Tokyo). This database includes the medical data of 684 people, which are with an average age of 64.5 (standard deviation: 6.1). The ratio between female and male is $65.2\% : 34.8\%$ and 47.6% of all participants have hypertension disease.

To find crossing points in these images (Fig. 2(a)–(d)), we used a segmentation model ([12]) to get vessel maps. We then classified each pixel on extracted vessels into artery/vein using [16]. We combine the vessel segmentation and classification results to find crossing points because classification results, which are more beneficial for crossing point detection, tend to have more errors while segmented vessel maps are more accurate. Therefore, we refine the classification results based on the vessel maps. A classic approach then finds crossing points in these refined artery/vein maps. Specifically, we find the artery pixels neighbouring vein pixels and check whether it is a crossing point or not using the skeletonized vessel map. The points marked in yellow in Fig. 2 are detected crossing point candidates. Note that for cup zones as indicated by a pink circle and dot in Fig. 2, we exclude candidates because the vessel system in this area is with high complexity and thus segmentation and classification are not reliable. Image patches are of size 150×150, centered at the crossing point candidates. Consequently, we detected $4,240$ crossing points and extracted corresponding image patches, centered at these crossing points.

Each image patch was carefully reviewed by a highly experienced ophthalmologist. Due to the errors in vessel segmentation and artery/vein classification, the detected crossing points may not be actual nor informative. Therefore, the specialist first annotated each image patch with a label on its validity, *i.e.*, if the image patch contains an actual and informative crossing point (*true*) or not (*false*). The numbers of true and false crossing points are $2,507$ and $1,733$, respectively. For each true crossing point, the specialist gave its severity label in $C = \{none, mild, moderate, severe\}$. The numbers of image patches with respective labels are $1,177$, 816, 457, and 57. In both the tasks, the datasets will be divided into training, validation, and test set following a ratio of 8:1:1. As an exameinee may have multiple retinal images, it is important to strictly put them into one same subset to prevent the training data contamination.

3   Severity Grading Pipeline

Our method forms a pipeline with three main modules, *i.e.*, preprocessing, patch validation, and severity grade prediction. The whole pipeline is shown in Fig. 2.
Preprocessing Steps (a)–(d) in the figure are preprocessing, in which the same processes as our dataset construction are applied to get image patches of 150×150 pixels with crossing point candidates.
Crossing Point Validation Both crossing point validation and severity grading are classification problems, whereas validation is easier because the label
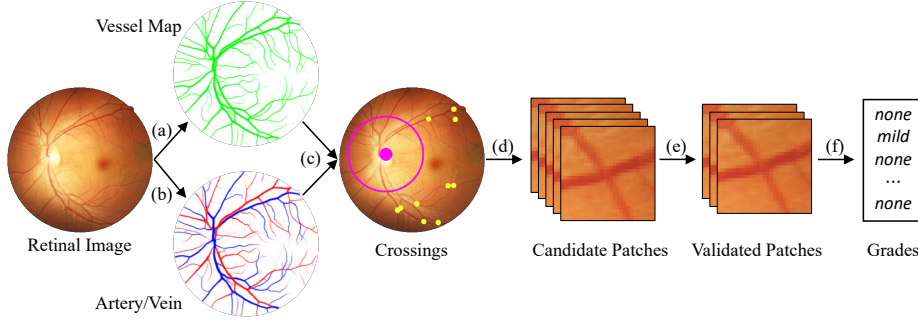
Fig. 2. Overall pipeline of our severity grading.

distribution is more balanced and the differences between real and false crossing points are more obvious. We find that commonly used classification models, such as [17,18,19], work well for our validation task (refer to Section 4).

Severity Grade Prediction The severity grade prediction task is much more challenging: Firstly, the label distribution is highly biased. For example, samples with the *none* label account for 68% of the total samples, while ones with the *severe* labels only take up 3%. Secondly, the difference among samples with different labels may not be clear enough. Even medical doctors may make diverse decisions on a single image patch.

For such classification tasks with ambiguous or imbalanced classes, the focal loss [15] has been used, which makes a model more aware of hard samples than easy ones. The focal loss introduces a hyperparameter γ, on which a model's performance depends significantly. Tuning this hyperparameter is extremely important yet computationally expensive [20]. A greater γ may make the model focus too much on hard samples, spoiling the accuracy on other samples, while a smaller γ may decrease its ability to classify hard samples.

We propose a multi-diagnosis team network (MDTNet) to address the aforementioned problems in severity grade prediction. As shown in Fig. 3, MDTNet consists of three modules, *i.e.*, a base module, a focal module, and a fusion module. The base and focal modules have multiple sub-models, and all of them take the same image patch as input. The difference between the sub-models in the base and focal modules is the losses: Ones in the base module adopt the cross entropy (CE) loss while ones in the focal module use the focal loss. These sub-models are trained independently with respective losses. The fusion module concatenates all features (*i.e.*, the outputs of the second last layers of the sub-models) into a single vector, which is then fed into two fully-connected layers to make the final prediction.

The focal loss is originally designed for object detection [15], defined as

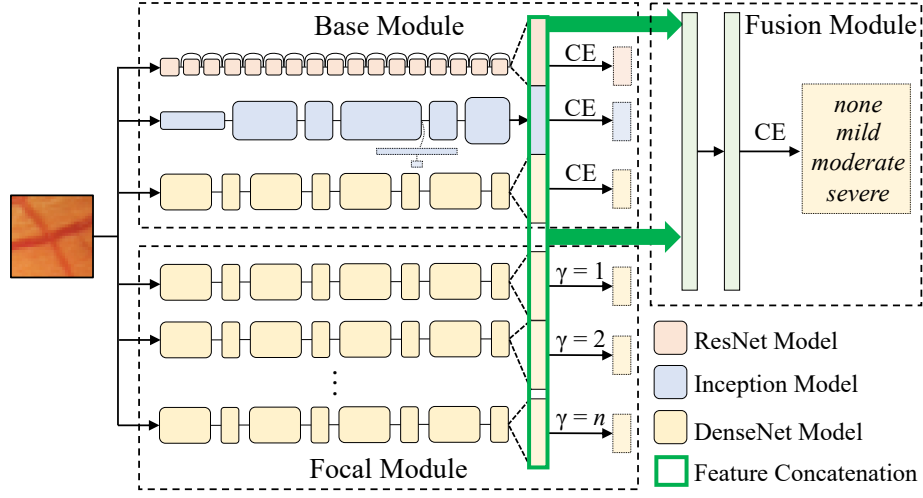$$L(y,t) = -\sum_l t_l (1 - y_l)^\gamma \log y_l, \tag{1}$$

Fig. 3. MDTNet for severity grade prediction.

where t is the one-hot representation of label and y is the softmax output from a model (t_l and y_l are the l-th entries of t and y); γ is a hyperparameter to weight hard examples. The focal loss reduces to the CE loss when $\gamma = 0$, and a larger γ weights more on hard examples. One possible criticism of the focal loss is its sensitivity to γ. We therefore propose to ensemble sub-models with different γ's. The hypothesis behind this choice is that different γ's may rely on different cues for prediction and aggregating respective features may help in improving the final decision. This is embodied in the focal module. The same idea can also be applied for different network architectures, embodied in the base module. These sub-models thus provide diagnostic features that may complement each other.

To cope with the imbalanced class distribution, we adopt class weighting [21,22]. We multiply weight $\alpha_l = \ln N_l / \ln N$ to each term (*i.e.* different l's) in the CE/focal loss, where N and N_l are the numbers of all samples and of samples with the label corresponding to the l-th entry of t. We pre-train the sub-models using their own classifiers and losses, and then freeze their weights to train the additional two fully-connected layers for the final decision.

Data Augmentation We adopt extensive data augmentation. During the training process, the input images have 50% chance to get each operator in Fig. 4. Among them, (b∼h) are used for shape modification, changing the locations and the shapes of the attention areas of the deep learning models; (i∼k) are to provide variety on imaging quality by blurring or adding random noises; (l) represents sensor characteristics of color (hue and saturation).
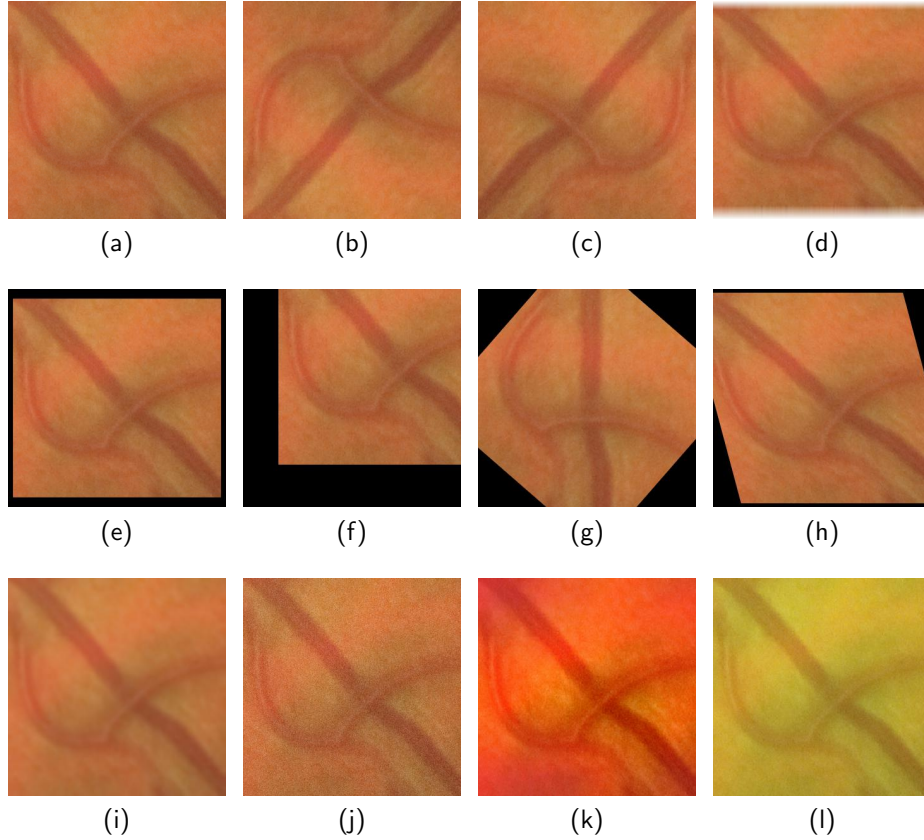
Fig. 4. Our data augmentation operator pool. (a) Raw image, (b) vertical flipping, (c) horizontal flipping, (d) cropping and padding, (e) scaling, (f) translating, (g) rotating, (h) sheering, (i) blurring, (j) additional noise, (k) additional frequency noise, and (l) color modification.

4   Experiments and Results

Implementation For sub-models in the base module, we used ResNet [17], Inception [19], and DenseNet [18]. In the focal module, DenseNet with $\gamma = 1$, 2, or 3 were used. All these models are pretrained over the ImageNet dataset [23]. The fully-connected layers in the fusion module are followed by the ReLU nonlinearity. For optimization, Adam [24] was adopted with a learning rate of 0.0001.

Performance of Base Models We first evaluated the performance of the base module's sub-models for the crossing point validation and severity grade prediction tasks. For comparison, we also give the results of models without pre-training (w/o PT) and without data augmentation (w/o DA), as well as models using only the green channel (GC Only).

Table 1. Performances of base models with ablation.

Models	Cross. Point Val.			Severity Grade Pred.		
	Pre.	Rec.	t (ms)	Acc.	Kappa	t (ms)
ResNet-50	0.9427	0.9526	0.274	0.8063	0.6629	0.278
—w/o PT	0.8646	0.6975	0.274	0.5445	0.0177	0.278
—w/o DA	0.9531	0.8551	0.274	0.5340	0.0036	0.278
—GC Only	0.9583	0.9154	0.273	0.7277	0.5288	0.273
Inception v3	0.9635	**0.9635**	0.218	0.8534	0.7432	0.222
—w/o PT	0.9010	0.6865	0.218	0.5183	0.0313	0.222
—w/o DA	0.9323	0.9179	0.218	0.5393	0.0000	0.222
—GC Only	0.9167	0.9119	**0.216**	0.8115	0.6771	**0.216**
DenseNet-121	0.9479	0.9630	0.266	**0.8795**	**0.7892**	0.269
—w/o PT	0.9375	0.6742	0.266	0.5288	0.0050	0.269
—w/o DA	**0.9740**	0.8274	0.266	0.7225	0.4865	0.269
—GC Only	**0.9740**	0.9212	0.266	0.6702	0.4406	0.267

Table 2. Performance of MDTNet models for severity grade prediction.

Metrics	DenseNet-121 (Focal Loss)				MDTNet		
	$\gamma = 1$	$\gamma = 2$	$\gamma = 5$	$\gamma = 10$	$n = 0$	$n = 1$	$n = 3$
Acc.	0.8639	0.7434	0.8639	0.7958	0.8953	0.9110	**0.9162**
Kappa.	0.7642	0.5685	0.7641	0.6508	0.8183	0.8453	**0.8542**
t (ms)	**0.268**	**0.268**	**0.268**	**0.268**	0.767	1.047	1.571

The crossing point validation performances are shown in the left part of Table 1. We use two metrics, precision and recall, and the time measurement to show the timing performance. We can see that pre-training and data augmentation can improve the overall performance of the crossing point validation. The Inception model with PT and DA achieved the best recall and the second-best precision. Note that PT and DA will not change the running time of the model because they do not modify the network structure.

The right part of Table 1 gives the results of the base models on the severity grade prediction task, and Table 2 presents the performance of MDTNet and models using the focal loss. In addition to the classification accuracy, we also adopt the Cohen's kappa, which can measure the agreement between the ground-truth labels and predictions. We can see that, compared with the focal loss models, the DenseNet can achieve higher overall accuracy with the CE loss. However, the combination among different models, different losses, as well as different γ values can boost the performance. MDTNet achieved the highest performance in this experiment when $n = 3$.

To better analyze the severity grade prediction performance, we present the confusion matrices in Fig. 5. It can be seen that, with the increment of the underlying sub-models, MDTNet gains the classification ability. Fig. 6 shows visual explanation of MDTNet by Grad-CAM [25]. Figs. 6 (a) and (b) show two examples for the crossing point validation. The ground-truth labels are *false* and the predictions were also *false*, *i.e.*, these are not effective crossing points as

Fig. 5. Confusion matrices for three different severity grade prediction models. The recall is shown in the last row and the precision is shown in the last column. (a) MDTNet without the focal module, (b) MDTNet for $n = 1$, and (c) MDTNet for $n = 3$.
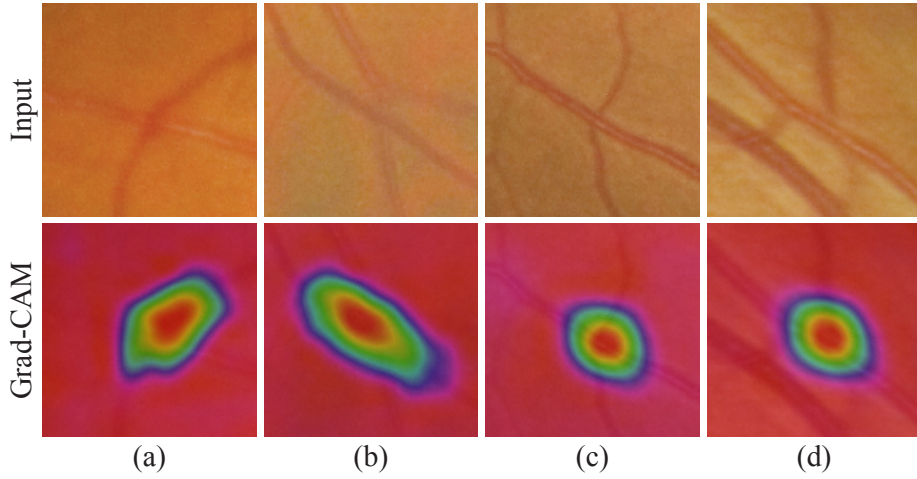

Fig. 6. Visual explanation of prediction results. (a,b) are for the crossing point validation model and (c,d) are from the severity grade prediction model. The first row is the raw input images and the second row is the class-discriminative regions.

the arteries are under the veins. The model mainly counted the red area in the second row along the vein. The model might find the vein, track it down, and reach to the conclusion that it lies above the artery. Figs. 6 (c) and (d) are for the severity grade prediction. The ground-truth labels are respectively *mild* and *moderate* and were both correctly predicted. We can see the artery runs over the vein deforming the vein. Being different from the example in (a) and (b), the model looks at the crossing points and looks for possible shape deformations and their extent.

5   Conclusion

The paper presents a method to automatically predict the arteriolosclerosis severity from retinal images. To improve the accuracy for ambiguous and unbalanced samples, we design the multi-diagnosis team network (MDTNet), which can jointly consider diagnostic cues from multiple sub-models, without tuning the hyperparameter for the focal loss. Experimental results show the superiority of our method, achieving over 91% accuracy.

6   Acknowledgements

7   Ethics Approval

This study was performed in accordance with the World Medical Association Declaration of Helsinki, and the study protocol was approved by the institutional review board of the Osaka University Hospital.

8   Conflict of Interest

Liangzhi Li, Manisha Verma, Bowen Wang, Yuta Nakashima, Ryo Kawasaki, and Hajime Nagahara have no conflicts of interest in association with this study.

References

1. I. P. Chatziralli, E. D. Kanonidou, P. Keryttopoulos, P. Dimitriadis, and L. E. Papazisis, "The value of fundoscopy in general practice," *The open ophthalmology journal*, vol. 6, p. 4, 2012.
2. L. D. Hubbard, R. J. Brothers, W. N. King, L. X. Clegg, R. Klein, L. S. Cooper, A. R. Sharrett, M. D. Davis, J. Cai, A. R. in Communities Study Group *et al.*, "Methods for evaluation of retinal microvascular abnormalities associated with hypertension/sclerosis in the atherosclerosis risk in communities study," *Ophthalmology*, vol. 106, no. 12, pp. 2269–2280, 1999.
3. J. B. Walsh, "Hypertensive retinopathy: Description, classification, and prognosis," *Ophthalmology*, vol. 89, no. 10, pp. 1127 – 1131, 1982.
4. U. T. V. Nguyen, A. Bhuiyan, L. A. F. Park, R. Kawasaki, T. Y. Wong, J. J. Wang, P. Mitchell, and K. Ramamohanarao, "An automated method for retinal arteriovenous nicking quantification from color fundus images," *IEEE Transactions on Biomedical Engineering*, vol. 60, no. 11, pp. 3194–3203, 2013.

5. S. Roychowdhury, D. D. Koozekanani, and K. K. Parhi, "Iterative vessel segmentation of fundus images," *IEEE Transactions on Biomedical Engineering*, vol. 62, no. 7, pp. 1738–1749, 2015.
6. J. U. Kim, H. G. Kim, and Y. M. Ro, "Iterative deep convolutional encoder-decoder network for medical image segmentation," in *IEEE Engineering in Medicine and Biology Society (EMBC)*, 2017, pp. 685–688.
7. Z. Yan, X. Yang, and K. Cheng, "Joint segment-level and pixel-wise losses for deep learning based retinal vessel segmentation," *IEEE Transactions on Biomedical Engineering*, vol. 65, no. 9, pp. 1912–1923, 2018.
8. F. Huang, B. Dashtbozorg, T. Tan, and B. M. ter Haar Romeny, "Retinal artery/vein classification using genetic-search feature selection," *Computer Methods and Programs in Biomedicine*, vol. 161, pp. 197 – 207, 2018.
9. M. I. Meyer, A. Galdran, P. Costa, A. M. Mendonça, and A. Campilho, "Deep convolutional artery/vein classification of retinal vessels," in *Image Analysis and Recognition*, 2018, pp. 622–630.
10. P. Costa, A. Galdran, M. I. Meyer, M. Niemeijer, M. Abràmoff, A. M. Mendonça, and A. Campilho, "End-to-end adversarial retinal image synthesis," *IEEE Transactions on Medical Imaging*, vol. 37, no. 3, pp. 781–791, 2018.
11. Y. Hatanaka, C. Muramatsu, T. Hara, and H. Fujita, "Automatic arteriovenous crossing phenomenon detection on retinal fundus images," in *Medical Imaging 2011: Computer-Aided Diagnosis*, vol. 7963, 2011, p. 79633V.
12. L. Li, M. Verma, Y. Nakashima, H. Nagahara, and R. Kawasaki, "IterNet: Retinal image segmentation utilizing structural redundancy in vessel networks," in *The IEEE Winter Conference on Applications of Computer Vision*, 2020, pp. 3656–3665.
13. V. B. S. Cambò, L. Cariello, and G. Mastronardi, "A combined method to detect retinal fundus features," in *IEEE European Conference on Emergent Aspects in Clinical Data Analysis*, 2005.
14. C. Taylor, A. J. Munro, R. Glynne-Jones, C. Griffith, P. Trevatt, M. Richards, and A. J. Ramirez, "Multidisciplinary team working in cancer: what is the evidence?" *The BMJ*, vol. 340, p. c951, 2010.
15. T. Lin, P. Goyal, R. Girshick, K. He, and P. Dollár, "Focal loss for dense object detection," *IEEE Transactions on Pattern Analysis and Machine Intelligence*, vol. 42, no. 2, pp. 318–327, 2020.
16. L. Li, M. Verma, Y. Nakashima, R. Kawasaki, and H. Nagahara, "Joint learning of vessel segmentation and artery/vein classification with post-processing," in *Medical Imaging with Deep Learning*, 2020.
17. K. He, X. Zhang, S. Ren, and J. Sun, "Deep residual learning for image recognition," in *The IEEE Conference on Computer Vision and Pattern Recognition (CVPR)*, 2016, pp. 770–778.
18. G. Huang, Z. Liu, G. Pleiss, L. Van Der Maaten, and K. Weinberger, "Convolutional networks with dense connectivity," *IEEE Transactions on Pattern Analysis and Machine Intelligence*, 2019.
19. C. Szegedy, V. Vanhoucke, S. Ioffe, J. Shlens, and Z. Wojna, "Rethinking the inception architecture for computer vision," in *The IEEE Conference on Computer Vision and Pattern Recognition (CVPR)*, 2016, pp. 2818–2826.
20. M. Weber, M. Fürst, and J. M. Zöllner, "Automated focal loss for image based object detection," *arXiv preprint arXiv:1904.09048*, 2019.
21. C. Huang, Y. Li, C. C. Loy, and X. Tang, "Learning deep representation for imbalanced classification," in *2016 IEEE Conference on Computer Vision and Pattern Recognition (CVPR)*, 2016, pp. 5375–5384.

22. Y. Cui, M. Jia, T.-Y. Lin, Y. Song, and S. Belongie, "Class-balanced loss based on effective number of samples," in *The IEEE Conference on Computer Vision and Pattern Recognition (CVPR)*, June 2019.

23. O. Russakovsky, J. Deng, H. Su, J. Krause, S. Satheesh, S. Ma, Z. Huang, A. Karpathy, A. Khosla, M. Bernstein, A. C. Berg, and L. Fei-Fei, "ImageNet Large Scale Visual Recognition Challenge," *International Journal of Computer Vision (IJCV)*, vol. 115, no. 3, pp. 211–252, 2015.

24. D. P. Kingma and J. Ba, "Adam: A method for stochastic optimization," *arXiv preprint arXiv:1412.6980*, 2014.

25. R. R. Selvaraju, M. Cogswell, A. Das, R. Vedantam, D. Parikh, and D. Batra, "Grad-cam: Visual explanations from deep networks via gradient-based localization," in *International Conference on Computer Vision (ICCV)*, 2017, pp. 618–626.